J Mater Sci: Mater Electron (2016) 27:8559–8566
DOI 10.1007/s10854-016-4873-y

Platinum nanoparticles supported on nitrogen and sulfur-doped reduced graphene oxide nanomaterial as highly active electrocatalysts for methanol oxidation

Onur Akyıldırım[1] · Haydar Yüksek[2] · Hasan Saral[3] · İsmail Ermiş[4] · Tanju Eren[5] · Mehmet Lütfi Yola[3]

Received: 21 March 2016 / Accepted: 19 April 2016 / Published online: 23 April 2016

Abstract A fuel cell is an electrochemical cell that converts a source fuel into an electrical current. It generates electricity inside a cell through reactions between a fuel and an oxidant, triggered in the presence of an electrolyte. Fuel cells have been attracting more and more attention in recent decades due to high-energy demands, fossil fuel depletions and environmental pollution throughout world. In this study, a facile and cost-effective catalysts have been developed on platinum nanoparticles (PtNPs) supported on nitrogen and sulfur-doped reduced graphene oxide (NSrGO). The successful synthesis of nanomaterials and the prepared glassy carbon electrode (GCE) surfaces were confirmed by transmission electron microscope (TEM), X-ray photo electron spectroscopy (XPS), scanning electron microscope (SEM) and electrochemical impedance spectroscopy (EIS). According to TEM images, the average particle sizes of PtNPs were found to be approximately 15–20 nm. The effective surface areas (ESA) of NSrGO/GCE and PtNPs/NSrGO/GCE were calculated to be 148 and 469 cm^2/mg, respectively. The PtNPs/NSrGO/GCE also exhibited a higher peak current for methanol oxidation than those of comparable GCE and NSrGO/GCE, providing evidence for its higher electro-catalytic activity.

✉ Haydar Yüksek
hyuksek61@gmail.com

✉ Mehmet Lütfi Yola
mehmetyola@gmail.com

[1] Department of Chemical Engineering, Faculty of Engineering and Architecture, Kafkas University, Kars, Turkey

[2] Department of Chemistry, Faculty of Science and Letters, Kafkas University, Kars, Turkey

[3] Department of Metallurgical and Materials Engineering, Faculty of Engineering, Sinop University, Sinop, Turkey

[4] Department of Energy System, Faculty of Engineering, Sinop University, Sinop, Turkey

[5] Department of Chemical Engineering, Faculty of Engineering, Pamukkale University, Denizli, Turkey

1 Introduction

Fuel cells can generate energy from various fuels and they are recently significant method in terms of electricity production. Especially, direct-methanol fuel cells (DMFCs) are proton-exchange fuel cell in which methanol is used as the fuel [1]. The important advantage of these fuel cells is the simplicity of transport of methanol. Methanol as fuel has several advantages such as transport and storage. DMFCs have been used for the production of energy for the several years [2]. A sulfuric acid or perchloric acid as supporting electrolyte is uses in the DMFCs owing to removing of the CO_2 during the electrochemical progress. The reaction of methanol oxidation in an acidic medium can be presented as below [3, 4]:

$$\text{(Anode) } CH_3OH + H_2O \rightarrow CO_2 + 6H^+ + 6e^- \quad E^\circ = 0.043 \text{ V (SHE)}$$

$$\text{(Cathode) } 3/2O_2 + 6H^+ + 6e^- \rightarrow 3H_2O \quad E^\circ = 1.229 \text{ V (SHE)}$$

(The all electrochemical reaction):

$$CH_3OH + 3/2O_2 \rightarrow CO_2 + 2H_2O \quad E^\circ = 1.186 \text{ V (SHE)}$$

Especially, various nanomaterials and nanoparticles based on electrodes can been utilized for the development of energy, sensor and catalytic effect. The chemically

modified electrodes in electrochemistry have been interesting research area in recent years. These electrodes are often prepared by modification of carbon or metal substrates to produce a new electrode to carry out specified reactions or processes. Modification of conductive substrates is also an important objective in material science and molecular electronics, as well as in various sensors applications. Recently, graphene, a carbon material, and nanoparticles modified electrodes have been prepared and various literatures have been reported for the determination of biological molecules with high sensitivity [2, 5–14]. Recently, graphene/graphene oxide has been considered as ''rising star" carbon material because of its unique properties, including superior mechanical strength [15], low density and high heat conductance [16]. In addition, some nanoparticles such as mono/bimetallic have important attention in nano/sensor technology [17]. The metal nanoparticles cause an increase in specific performances such as electronic and catalytic effects and create synergetic effects because the nano-sized particles have larger specific surface area, they are good catalysts. In addition, the nanoparticles can increase the rate of electrochemical reaction [18].

In the present report, the preparation and characterization of PtNPs/NSrGO nanocomposite were performed (Scheme 1). After that, glassy carbon electrode (GCE) surfaces were modified with PtNPs/NSrGO nanocomposite by using infrared heat lamp. The developed surfaces were characterized by EIS, cyclic voltammetry (CV) and chronoamperometry (CA) measurements. After the characterizations of the glassy carbon surfaces, these catalysts were investigated their effects in fuel cell applications.

2 Experimental

2.1 Materials

All chemicals that used in the experiments were reagent grade and were used as received following; graphite powder (Merck, Germany), sulfuric acid (H_2SO_4, Merck, Germany), potassium persulfate ($K_2S_2O_8$, Merck, Germany), phosphorus pentoxide (P_2O_5, Merck, Germany), potassium permanganate ($KMnO_4$, Merck, Germany), hydrogen peroxide (H_2O_2, Merck, Germany), ethanol (Merck, Germany), hydrochloric acid (HCl, Sigma-Aldrich), ethanol (Sigma-Aldrich, USA), chloroplatinic acid (H_2PtCl_6, Sigma-Aldrich, USA), isopropyl alcohol (IPA, Sigma-Aldrich, USA), methanol (Merck, Germany), HPLC grade acetonitrile (MeCN, Sigma-Aldrich, USA), $NaBH_4$ (Merck, Germany), perchloric acid ($HClO_4$, Sigma-

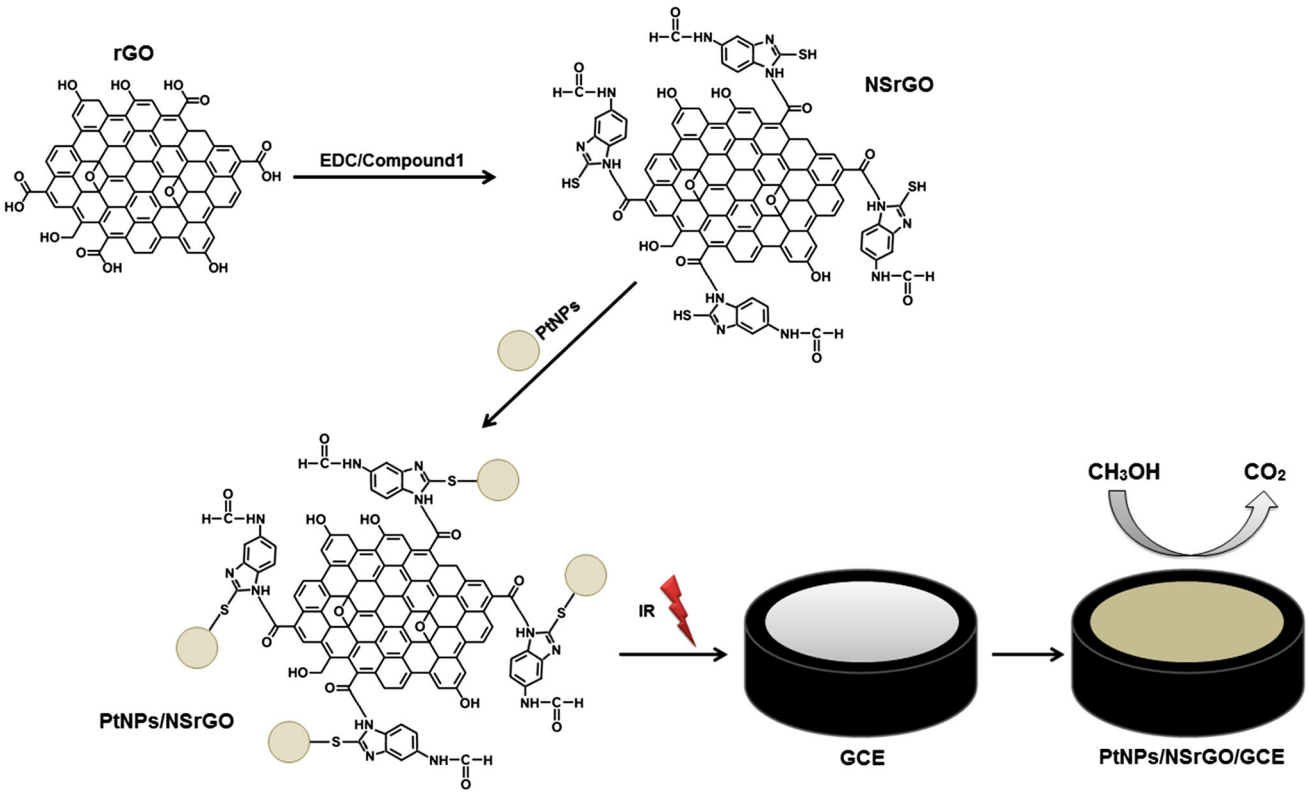

Scheme 1 The procedure of fabrication of the catalysts in present study

Scheme 2 Synthesis route of compound 1

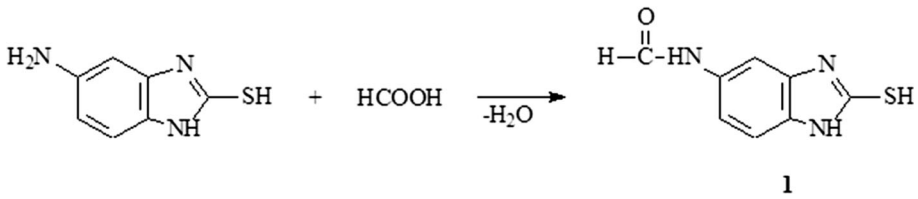

Aldrich, USA), and other chemicals were reagent grade quality and were used as received.

2.2 Instrumentation

All electrochemical experiments (CV and CA) were performed using out IviumStat (US) equipped with C3 cell stand. Electrochemical impedance spectroscopic experiments were carried out with a Gamry Reference 600 workstation equipped with a PCI4/300 potentiostat in conjunction with EIS 300 software. Modified electrodes were characterized in 1.0 mM ferrocyanide/1.0 mM ferricyanide ($[Fe(CN)_6]^{3-/4-}$) redox couple via EIS methods. EIS data were measured at 100 kHz to 0.1 Hz at 10 mV wave amplitude and at an electrode potential of 0.150 V, the formal potential of $[Fe(CN)_6]^{3-/4-}$ redox couple. Argon gas was passed through the solutions during experiments for about 10 min. JEOL 2100 HRTEM (JEOL Ltd., Tokyo, Japan) and ZEISS EVO 50 SEM (GERMANY) analytic microscopies were used to investigate the morphologies of the nanocomposites. XPS analysis were performed on a PHI 5000 Versa Probe (F ULVAC-PHI, Inc., Japan/USA) model with monochromatized Al Ka radiation (1486.6 eV) as an X-ray anode operated at 50 W. To prepare the samples, one drop of the prepared nanocomposites were placed on clear glass and then dried in air.

Melting point was determined in open glass capillary using a Stuart melting point SMP30 apparatus and is uncorrected. The IR spectra were obtained on an ALPHA-P BRUKER FT-IR spectrometer. 1H and 13C NMR spectra were recorded in deuterated dimethyl sulfoxide with TMS as internal standard using a Varian spectrometer at 400 and 100 MHz, respectively.

2.3 General procedure for the synthesis of compound 1 (for nitrogen and sulfur-functionalized reduced graphene oxide)

5-Amino-2-mercaptobenzimidazole (0.01 mol) was treated with formic acid (0.01 mol), and then the mixture was refluxed for 5 h and filtered [19]. The filtrate was evaporated in vacuo and the crude product was recrystallized from ethanol to afford compound 1. Yield: 1.81 g (94 %); mp: 311 °C; IR (KBr, υ, cm^{-1}): 3131 (NH), 2849 and 2789 (CHO), 2555 (SH), 1716 (C=O); 1H NMR (400 MHz, DMSO-d6): δ 7.04 (d, 1H, Ar–H, J = 8.55 Hz), 7.13 (d, 1H, Ar–H, J = 6.72 Hz), 7.68 (s, 1H, Ar–H), 10.19 (s, 1H, CHO), 12.42 (s, 1H, SH), 12.45 (s, 1H, 2NH); 13C NMR (100 MHz, DMSO-d6): δ 101.32 (arom-C), 110.14 (arom-C), 114.49 (arom-C), 129.11 (arom-C), 133.01 (arom-C), 134.27 (arom-C), 160.07 (CHO), 168.86 (C-SH) (Scheme 2).

2.4 Preparation of NSrGO and PtNPs/NSrGO nanohybrids

Graphene oxide (GO) was synthesized according to our previous report [10, 20]. The as-prepared GO was dispersed into 200 mL water under mild ultrasound yielding a yellow–brown suspension, then 4 mL hydrazine hydrate (80 wt%) were added and the solution was heated in an oil bath maintaining at 100 °C under a water-cooled condenser for 24 h. After the reaction, the prepared rGO product was collected by vacuum filtration. rGO was dissolved in ethanol at 2 mg mL^{-1}. The mixture was sonicated to form a homogeneous suspension. The prepared rGO suspension was treated with 0.2 M of EDC solution for 8 h to ensure the surface activation of residual carboxylated groups. EDC compound provides the most popular and versatile method for labeling or crosslinking to free carboxylic groups on rGO. The EDC molecules are considered zero-length carboxyl-to-amine crosslinkers. EDC reacts with carboxylic acid groups to form an active intermediate product that is easily displaced by nucleophilic attack from primary amino groups in the reaction mixture. The primary amine forms an amide bond with the original carboxyl group, and an EDC by-product is released as a soluble derivative. Therefore, we used EDC for activation of free carboxylic acid groups of rGO. Then 1.0 mM of compound 1 was mixed with the activated rGO suspension at a 1:1 volume ratio and kept stirring for 2 h (NSrGO).

PtNPs were prepared by mixing 200 μL of 0.1 M K_2PtCl_4 solution with 10 mg $NaBH_4$ solution. The solutions were kept in ultra-sonicated bath for 60 min [21]. After that, 1 mg mL^{-1} of PtNPs solution was mixed with the 0.1 mg mL^{-1} of NSrGO solution at a 1:1 volume ratio. Finally, the mixture was sonicated to generate a homogeneous mixture (PtNPs/NSrGO). The mixture was then kept undisturbed under ambient condition for 24 h.

2.5 Procedure for the electrode preparation

GCE was cleaned according to our previous reports [22] and used as a working electrode. After that, the catalyst inks were prepared by dispersing 1 mg of catalyst (NSrGO and PtNPs/NSrGO) into 1 mL of ethanol via 20 min agitation. 15 μL of NSrGO and PtNPs/NSrGO suspensions was dropped onto the clean GCE surfaces. Then, the solvent was evaporated by an infrared lamp.

2.6 Electrochemical measurements

Electrocatalytic oxidation of 0.5 mol L^{-1} methanol on bare GCE, NSrGO/GCE and PtNPs/NSrGO/GCE was performed in 0.1 mol L^{-1} $HClO_4$ by cyclic voltammetry (CV) between 0.0 and +1.2 V. The Ag/AgCl and Pt wire electrodes were utilized as reference and counter electrode, respectively.

3 Results and discussion

3.1 Characterization of nanomaterials

The morphologies of the rGO and PtNPs/NSrGO nanohybrid were investigated by using the JEOL 2100 HRTEM with an accelerating voltage of 200 keV. A drop of sample solution was deposited on a polymeric grid at room temperature under an argon gas stream. Figure 1a shows the shows the transparent, creased and planar sheet like morphology of rGO. Figure 1b confirms that the PtNPs have been seen as dark dots with a mean diameter of 15–20 nm on NSrGO sheets.

SEM characterization was performed to evaluate the morphologies of the surfaces. Figure 2a shows the smooth surface of bare GCE. After the modification of GCE with NSrGO nanocomposite, some layers were observed on NSrGO/GCE in Fig. 2b. The SEM graph of PtNPs/NSrGO

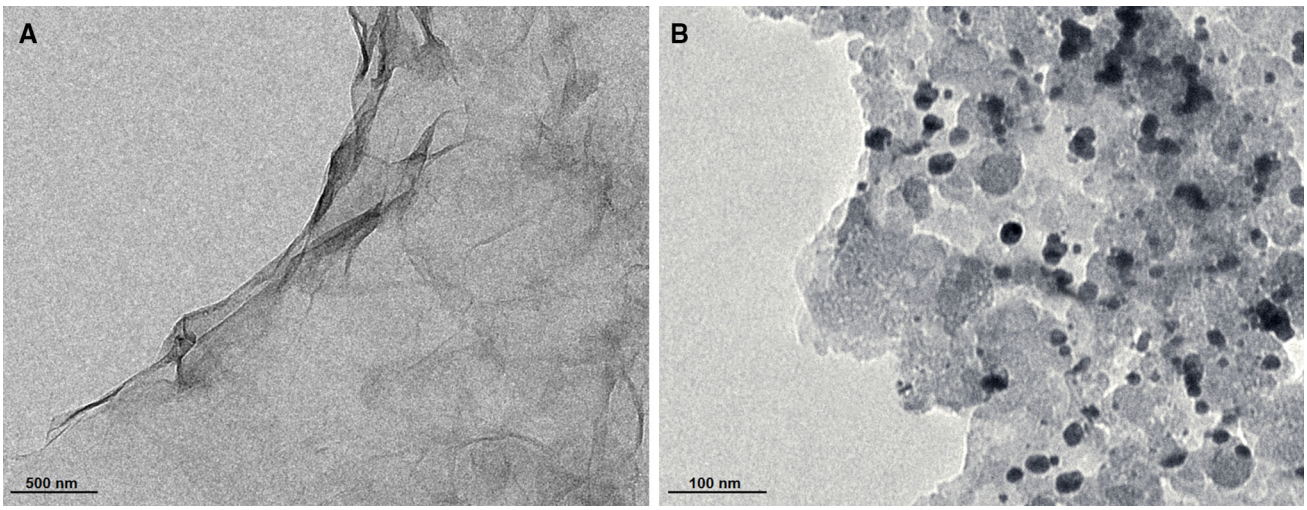

Fig. 1 TEM image of **a** rGO and **b** PtNPs/NSrGO

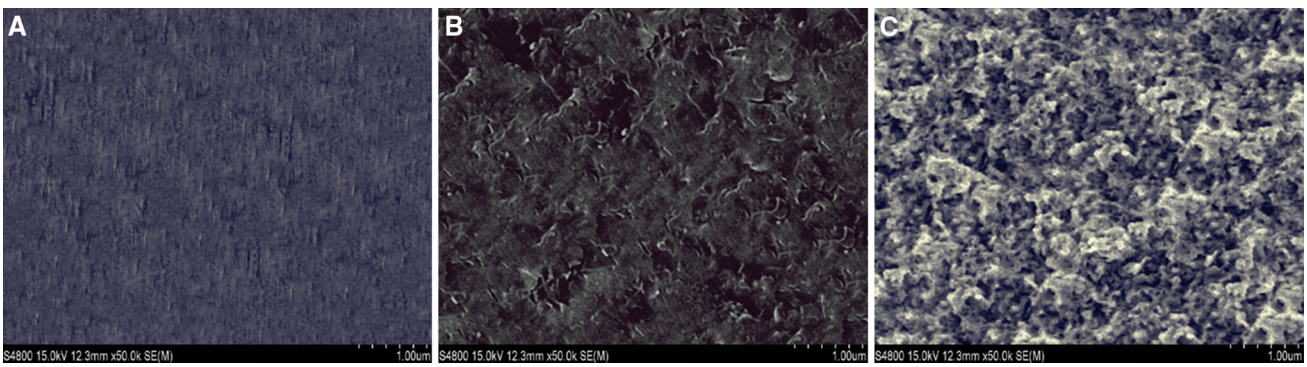

Fig. 2 SEM image of **a** bare GCE; **b** NSrGO/GCE and **c** PtNPs/NSrGO/GCE

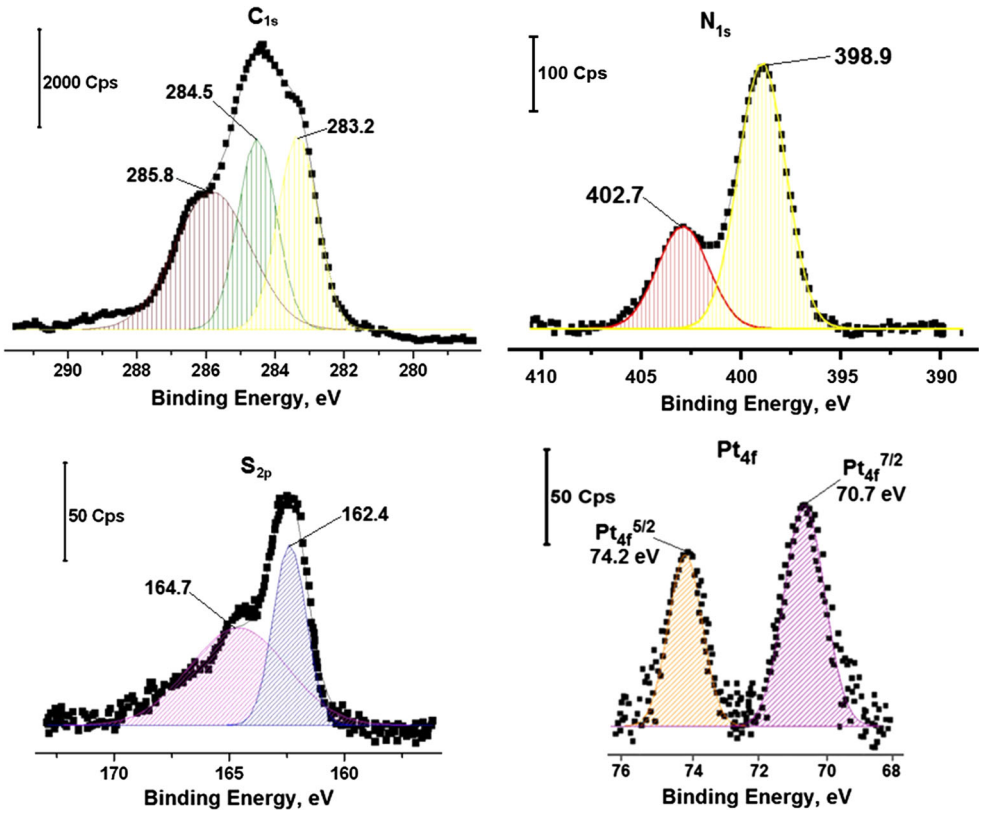

Fig. 3 The narrow region XPS of C1s, N1s and S2p of NSrGO and Pt4f of PtNPs/NSrGO

on GCE indicated that after the modification of PtNPs on NSrGO, a shiny intensive layer was observed covering the surface (Fig. 2c).

Figure 3a shows narrow region XPS spectra of NSrGO nanocomposite. As seen in Fig. 3a; C1s, N1s, and S2p peaks of NSrGO confirmed that rGO structure was functionalized with thiol group. The peaks at 283.2, 284.5 and 285.8 eV were related to C–C/C=C, C=O and C–N of C1s, respectively. The peak at 398.9 eV in the N1s narrow region spectrum was corresponded to C–N groups in the covalent attachment of nitrogen group to the rGO. The peak at 402.7 eV was corresponded to the N–H group in unreacted molecules. The doublet 4f5/2 and 4f7/2 signals of Pt4f region appeared at 74.3 and 70.4 eV, respectively, indicated the presence of PtNPs on NSrGO.

3.2 Characterizations of modified glassy carbon electrodes by EIS

EIS is an effective method for probing the features of surface modified electrodes. It is capable of giving useful information about defects/holes exist on the modified surfaces, the kinetics and mechanism of the film formation processes and surface coverage [22, 23]. Figure 4 shows the impedance plot (Nyquist diagram) of bare GCE, NSrGO/GCE and PtNPs/NSrGO/GCE. In addition, the

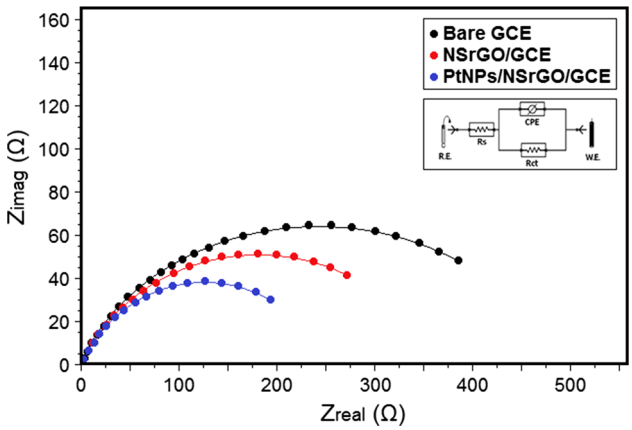

Fig. 4 Fitting of impedance spectrum for 1.0 mM $[Fe(CN)_6]^{3-/4-}$ (1:1) in 0.1 M KCl at bare GCE; NSrGO/GCE and PtNPs/NSrGO/GCE: *Insert* is the Randles equivalent circuit for PtNPs/NSrGO. Frequency range is 100,000–0.1 Hz with 10 mV wave amplitude at a formal potential of 0.150 V. *RE* stands for reference electrode and *WE* for working electrode

inset of Fig. 5 shows the experimental data that are fitted to standard Randles equivalent circuits for PtNPs/NSrGO/GCE surface analysis, which comprises the solution resistance (R_s), the charge transfer resistance (R_{ct}) and the constant phase element (CPE) for the cases of PtNPs/NSrGO/GCE. The experimental impedance values are

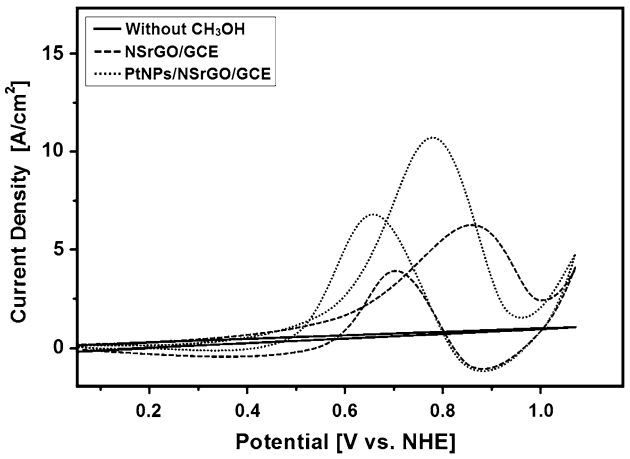

Fig. 5 Cyclic voltammograms of 0.5 mol L^{-1} methanol in 0.1 mol L^{-1} $HClO_4$ at bare GCE, NSrGO/GCE and PtNPs/NSrGO/GCE

matched with Randles equivalent circuit simulation using Gamry software (EIS 300 Electrochemical Impedance Spectroscopy Software). The EIS graph (Fig. 4) demonstrated that the value of charge transfer resistance (R_{ct}) of bare GCE was calculated as 460 Ω for $[Fe(CN)_6]^{3-/4-}$ redox couple solution. When the bare GCE was modified with NSrGO, the value of R_{ct} was lower (350 Ω). Because of the lower value, we can say that the NSrGO facilitated the rate of electron transfer between surface and solution. When NSrGO nanocomposite was modified with PtNPs, the value of R_{ct} of PtNPs/NSrGO/GCE was lower than that of NSrGO/GCE. According to the lower values of R_{ct}, PtNPs/NSrGO facilitated the rate of electron transfer in comparison to only NSrGO film. Thus, the addition of Pt nanoparticle shows the more increase of catalytic activity, indicating the more active property of the PtNPs/NSrGO film.

The ESA of different modified electrodes was obtained by CV with 1.0 mM $[Fe(CN)_6]^{3-}$ solution containing 0.1 M KCl as a probe at different scan rates according to the equation: $i_p = 2.69 \times 10^5\ A\ n^{3/2}\ D^{1/2}\ C\ v^{1/2}$, where i_p refers to the peak current and A is the electrode area (cm^2). For 1.0 mM $[Fe(CN)_6]^{3-}$, n = 1, D = 7.6×10^{-6} $cm^2\ s^{-1}$ (0.1 M KCl), C is the concentration of $[Fe(CN)_6]^{3-}$, v is the scan rate. The ESA of NSrGO/GCE and PtNPs/NSrGO/GCE were calculated from the slope of the i_p versus $v^{1/2}$ plot to be 148 cm^2/mg, and 469 cm^2/mg, respectively. These results show that the electrochemical surface area of the PtNPs/NSrGO/GCE is 3.17 times higher than those of NSrGO/GCE. The high activity was explained by the small size of PtNPs.

The electrocatalytic activities of the modified electrodes were also evaluated for 0.5 M methanol by CV in 0.1 mol L^{-1} $HClO_4$ at 50 mV s^{-1} (Fig. 5). In the case of the PtNPs/NSrGO/GCE, a current peak of 11.2 ± 0.06 A cm^{-2} was observed during a forward anodic scan (If) at a potential of 0.80 V, while the reverse scan (Ib) showed a current peak of 5.17 ± 0.03 A cm^{-2} at 0.65 V. The efficiencies of the PtNPs/NSrGO/GCE and NSrGO/GCE on methanol oxidation were given in Table 1. The forward peak of PtNPs/NSrGO/GCE was 2.20 times higher than those of NSrGO/GCE. In addition, a control experiment of the PtNPs/NSrGO/GCE in the electrolyte without methanol was completed (black curve of Fig. 5). According to the black curve, during the forward anodic scan and the reverse scan, no current peak was seen. Thus, the important activity enhancement in methanol oxidation is attributed to high active surface and effective electronic interactions between PtNPs and NSrGO nanocomposite [24].

In addition, since the anodic peak in the backward scan was related to the removal of CO accumulated on the catalyst surface during the forward scan, the ratio of If/Ib (the ratio of the forward and backward anodic peak current densities) can be used to evaluate the CO tolerance of catalysts [1]. A higher If/Ib ratio indicates the more effective removal of poisoning CO species on catalyst surface. The If/Ib ratio of PtNPs/NSrGO/GCE was 2.16, higher than the 2.04 for the NSrGO/GCE. These electrochemical results reveal that the PtNPs/NSrGO/GCE catalyst has better CO-poisoning tolerance and high electrocatalytic activity toward methanol oxidation.

Figure 6 shows that the current density is proportional to the square root of the scan rate. This indicates that the electrochemical oxidation of methanol is diffusion processes at all surfaces. The slope for PtNPs/NSrGO/GCE is larger than those for the other modified GCE. Thus, we can say that the diffusion process of methanol is fastest on the PtNPs/NSrGO/GCE.

The chronoamperometry measurements were carried out to investigate the electrochemical performances of the prepared electrodes at 0.6 V in the presence of methanol. As shown in Fig. 7, all electrodes present current decay before steady current status is attained. The decay is possibly attributed to the fact that once the methanol oxidation reaction begins, some incomplete oxidation products

Table 1 Comparison of methanol oxidation on modified electrodes in this study (n = 6) (Scan rate: 50 mV s^{-1})

Electrode	If (A cm^{-2})	E (V)	Ib (A cm^{-2})	E (V)	If/Ib
PtNPs/NSrGO/GCE	11.2 ± 0.06	0.80	5.17 ± 0.03	0.65	2.16
NSrGO/GCE	5.1 ± 0.05	0.85	2.5 ± 0.04	0.70	2.04

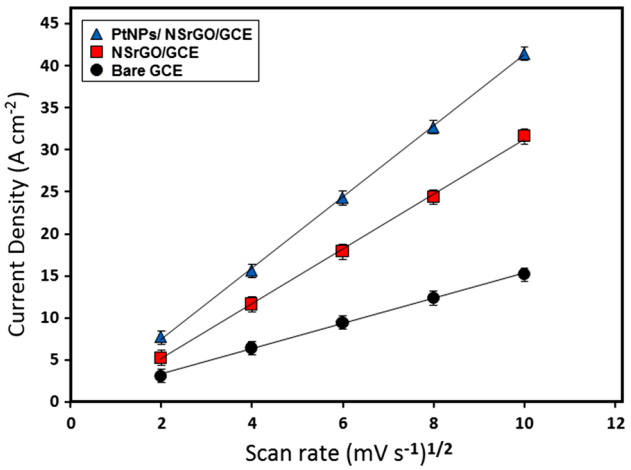

Fig. 6 The relationship of current density versus the square root of scan rate at bare GCE, NSrGO/GCE and PtNPs/NSrGO/GCE

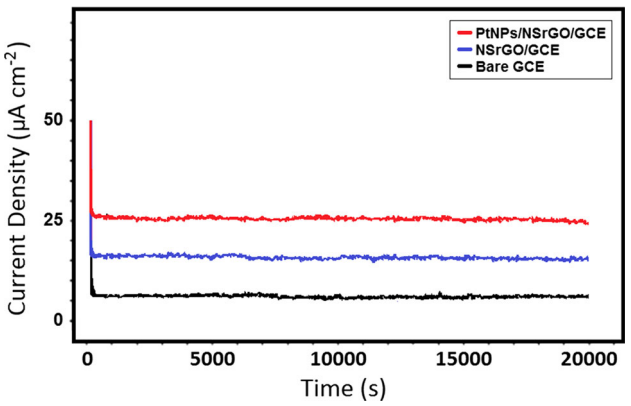

Fig. 7 Chronoamperometry results of 0.5 mol L^{-1} methanol in 0.1 mol L^{-1} $HClO_4$ at bare GCE, NSrGO/GCE and PtNPs/NSrGO/GCE

adsorb on the catalyst surface and poison it towards further methanol oxidation, which can also been observed in other studies [2, 25]. In the steady-state region, the current density of methanol oxidation on the PtNPs/NSrGO/GCE is highest than that of methanol oxidation on the other electrodes. This indicates that the PtNPs/NSrGO/GCE is a stable and poisoning-tolerance electrocatalyst for methanol oxidation.

3.3 The comparisons with the previous catalysts in the literature

Bimetallic core–shell Ag@PtNPs attached on multiwall carbon nanotube was synthesized. In addition, Pt-MWNT and Pt-C under the same amount of Pt loading (5 μg) were prepared [1]. In the case of the Ag@Pt-MWNT, a current peak of 1.58 A cm^{-2} was observed during a forward anodic scan at a potential of 0.92 V, while the reverse scan produced a current peak of 1.22 A cm^{-2} at 0.71 V. The forward peak was 7.09 and 12.15 times higher than those of Pt-MWNT and Pt-C samples. According to the results, the performance of the PtNPs/NSrGO is higher than those of the mentioned surfaces (Table 1).

The bimetallic Au–Pt alloyed nanochains supported on reduced graphene oxide (Au–Pt NCs/rGO) were prepared for DMFCs [26]. 3 mg of the sample was dispersed into 1 mL of water and ultrasonicated for 30 min to obtain a homogeneous suspension. Then, 6 mL of the suspension was uniformly casted on the GCE surface. The ESA was calculated to be 324.3 cm^2/g for Au–Pt NCs/rGO, which is not larger than that of PtNPs/NSrGO (469.0 cm^2/mg).

Ma et al. [27] prepared reduced graphene oxide (rGO) modified with 1,10-dimethyl-4,40-bipyridinium dichloride (methyl viologen, MV). After that, they performed immobilization of Pt nanoparticles to prepare a Pt/MV–rGO catalyst for direct methanol fuel cells. The ESA values of Pt/MV–rGO (5 mg) and Pt/rGO (5 mg) were estimated to be 246.5 and 82.5 cm^2/g, respectively, indicating more lower than PtNPs/NSrGO (469.0 cm^2/mg).

Pt-SiO_2/graphene nanocomposites (Pt-SiO_2-G) have been synthesized under solvothermal conditions [28]. The If/Ib value of Pt-SiO_2-G (5 mg) was estimated to be 1.04, indicating that the best catalyst in this study shows more electrocatalytic activity toward methanol oxidation.

4 Conclusions

A new and cost-effective catalysts based on platinum nanoparticles using a minimal amount of the precious metal was developed for the production of a working electrode that can be utilized in DMFCs. The catalysts were successfully prepared and modified on GCE surfaces in the present study. The PtNPs/NSrGO/GCE catalyst was well characterized in terms of TEM, SEM and XPS results. According to the results of EIS and CV, the prepared nanocomposites based on platinum nanoparticles showed catalytic activity towards methanol as the fuel. Especially, the PtNPs/NSrGO/GCE catalyst provides an opportunity to prepare a promising electrode with a large active surface area of 469.0 cm^2/mg, high electro-oxidative activity and superior CO tolerance than the NSrGO/GCE catalysts. In addition, the performance of the PtNPs/NSrGO/GCE catalyst is higher than those of catalysts in the mentioned literatures such as current densities on forward anodic scan and the reverse scan, the ratio of the forward and backward anodic peak current densities.

References

1. M. Rashid, T.-S. Jun, Y. Jung, Y.S. Kim, Sens. Actuators, B **208**, 7–13 (2015)
2. N. Atar, T. Eren, M.L. Yola, H. Karimi-Maleh, B. Demirdogen, RSC Adv. **5**, 26402–26409 (2015)
3. F. Şen, G. Gökağaç, J. Phys. Chem. C **111**, 5715–5720 (2007)
4. F. Şen, G. Gökağaç, J. Phys. Chem. C **111**, 1467–1473 (2007)
5. M.L. Yola, N. Atar, Electrochim. Acta **119**, 24–31 (2014)
6. H. Karimi-Maleh, P. Biparva, M. Hatami, Biosens. Bioelectron. **48**, 270–275 (2013)
7. H.K. Maleh, F.T. Javazmi, A.A. Ensafi, R. Moradi, S. Mallakpour, H. Beitollahi, Biosens. Bioelectron. **60**, 1–7 (2014)
8. A.A. Ensafi, H.K. Maleh, J. Electroanal. Chem. **640**, 75–83 (2010)
9. M.R. Shahmiri, A. Bahari, H.K. Maleh, R. Hosseinzadeh, N. Mirnia, Sens. Actuators, B **177**, 70–77 (2013)
10. R. Moradi, S.A. Sebt, H.K. Maleh, R. Sadeghi, F. Karimi, A. Bahari, Phys. Chem. Chem. Phys. **15**, 5888–5897 (2013)
11. A.A. Ensafi, H.K. Maleh, S. Mallakpour, M. Hatami, Sens. Actuators, B **155**, 464–472 (2011)
12. H. Beitollah, M. Goodarzian, M.A. Khalilzadeh, H.K. Maleh, J. Mol. Liq. **173**, 137–143 (2012)
13. E. Afsharmanesh, H.K. Maleh, A. Pahlavan, J. Vahedi, J. Mol. Liq. **181**, 8–13 (2013)
14. N. Atar, T. Eren, M.L. Yola, H. Gerengi, S. Wang, Ionics **21**, 3185–3192 (2015)
15. B.J. Sanghavi, W. Varhue, J.L. Chávez, C.-F. Chou, N.S. Swami, Anal. Chem. **86**, 4120–4125 (2014)
16. S. Stankovich, D.A. Dikin, G.H.B. Dommett, K.M. Kohlhaas, E.J. Zimney, E.A. Stach, R.D. Piner, S.T. Nguyen, R.S. Ruoff, Nature **442**, 282–286 (2006)
17. V.K. Gupta, N. Atar, M.L. Yola, Z. Üstündağ, L. Uzun, Water Res. **48**, 210–217 (2014)
18. B.J. Sanghavi, G. Hirsch, S.P. Karna, A.K. Srivastava, Anal. Chim. Acta **735**, 37–45 (2012)
19. S.A.F. Rostom, M.A. Shalaby, M.A. El-Demellawy, Eur. J. Med. Chem. **38**, 959–974 (2003)
20. N. Atar, M.L. Yola, T. Eren, Appl. Surf. Sci. **362**, 315–322 (2016)
21. G. Yang, Y. Zhou, H.-B. Pan, C. Zhu, S. Fu, C.M. Wai, D. Du, J.-J. Zhu, Y. Lin, Ultrason. Sonochem. **28**, 192–198 (2016)
22. M.L. Yola, N. Atar, M.S. Qureshi, Z. Üstündağ, A.O. Solak, Sens. Actuators, B **171**, 1207–1215 (2012)
23. V.K. Gupta, M.L. Yola, N. Atar, A.O. Solak, L. Uzun, Z. Üstündağ, Electrochim. Acta **105**, 149–156 (2013)
24. L. Su, W. Jia, C.-M. Li, Y. Lei, Chem. Sus. Chem. **7**, 361–378 (2014)
25. Y.Y. Tong, C.D. Gu, J.L. Zhang, M.L. Huang, H. Tang, X.L. Wang, J.P. Tu, J. Mater. Chem. A **3**, 4669–4678 (2015)
26. D.J. Chen, Q.L. Zhang, J.X. Feng, K.J. Ju, A.J. Wang, J. Wei, J.J. Feng, J. Power Sources **287**, 363–369 (2015)
27. J. Ma, L. Wang, X. Mu, Y. Cao, J. Colloid Interface Sci. **457**, 102–107 (2015)
28. T.H.T. Vu, T.T.T. Tran, H.N.T. Le, L.T. Tran, P.H.T. Nguyen, H.T. Nguyen, N.Q. Bui, Electrochim. Acta **161**, 335–342 (2015)